LA-13188-T
Thesis

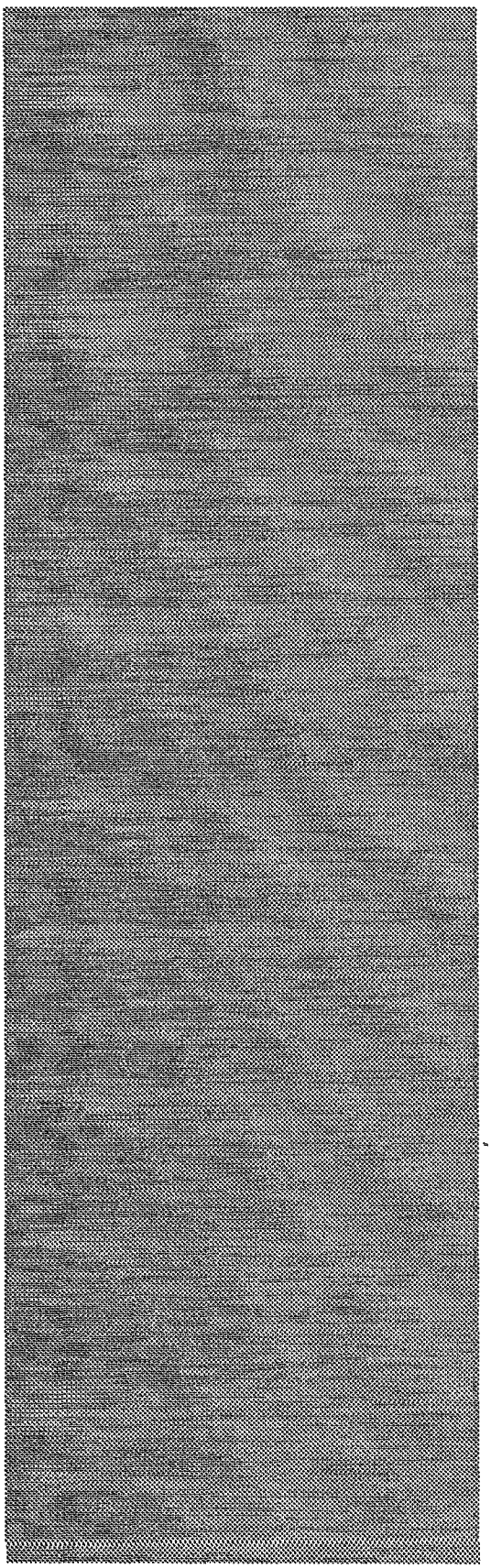

A Kinetic Study of Plutonium Dioxide Dissolution in Hydrochloric Acid Using Iron (II) as an Electron Transfer Catalyst

Los Alamos
NATIONAL LABORATORY

Los Alamos National Laboratory is operated by the University of California for the United States Department of Energy under contract W-7405-ENG-36.

This thesis was accepted by the Graduate School, New Mexico State University, Las Cruces, New Mexico, in partial fulfillment of the requirements for the degree of Doctor of Philosophy specializing in Chemical Engineering. The text and illustrations are the independent work of the author and only the front matter has been edited by the CIC-1 Writing and Editing Staff to conform with Department of Energy and Los Alamos National Laboratory publication policies.

An Affirmative Action/Equal Opportunity Employer

LA-13188-T
Thesis

UC-701
Issued: September 1996

A Kinetic Study of Plutonium Dioxide Dissolution in Hydrochloric Acid Using Iron (II) as an Electron Transfer Catalyst

Keith William Fife

Los Alamos
NATIONAL LABORATORY
Los Alamos, New Mexico 87545

ACKNOWLEDGMENTS

This program has taken the better part of five years to complete and has been successfully integrated into a full-time career. I must thank the management and technical staff of the Nuclear Materials Technology Division at Los Alamos National Laboratory for their support of this degree program. They not only provided the fundamental opportunity for this investigation, but they provided all financial support, mentor opportunities, and the laboratory facilities to accomplish this work.

I especially thank Wayne H. Smith for his help in understanding and troubleshooting the electrochemical systems as well as for many helpful discussions and comments, to Louis D. Schulte for his continued interest and helpful discussions regarding this research topic, to Gregory D. Bird and Charles C. Davis for their operation of the LASENTEC LAB-TEC™ 1000 instrument performing the transit time measurements of PuO_2 particle size distribution and surface area, to Michael D. Greenbank for all photography, and to Robert F. Meehan for the electronic versions of the cyclic voltammograms. Also to be recognized for their support are Dana C. Christensen, Joel D. Williams, and Stephen L. Yarbro (all soon to complete their doctorates) for pursuing this degree program in this manner.

The Department of Chemical Engineering at NMSU is to be recognized for their open support and vision; not only for this work, but for taking the chance to initiate and develop this novel distance learning program for which I am proud to have been a part. Key in originally initiating and developing this program is Dr. Stanford T. Holbrook.

And for the gracious use of Fig. 2.1b and Fig. 2.2 in this text, the American Chemical Society is acknowledged.

TABLE OF CONTENTS

LIST OF TABLES

LIST OF APPENDIX TABLES

LIST OF FIGURES

LIST OF APPENDIX FIGURES

A KINETIC STUDY OF PLUTONIUM DIOXIDE DISSOLUTION IN HYDROCHLORIC ACID USING IRON (II) AS AN ELECTRON TRANSFER CATALYST

BY

KEITH WILLIAM FIFE

ABSTRACT

Effective dissolution of plutonium dioxide has traditionally been accomplished by contact with strong nitric acid (>8 *M*) containing a small amount of fluoride (<0.5 *M*) at temperatures of ~100°C. In spite of these aggressive conditions, PuO_2 dissolution is sometimes incomplete requiring additional contact with the solvent.

This work focused on an alternative to conventional dissolution in nitric acid where an electron transfer catalyst, Fe(II), was used in hydrochloric acid. The overall dissolution reaction appeared to proceed according to the following:

$$PuO_2 + 4H^+ + Fe^{+2}_{(aq)} \rightarrow Pu^{+3}_{(aq)} + 2H_2O + Fe^{+3}_{(aq)}$$

The work was an extension of an earlier investigation (Shakila et al. 1989), and used bulk electrolysis to maintain iron in the reduced state for continued reaction with the plutonium oxide surface. Cyclic voltammetry was employed as an *in-situ* analytical technique for monitoring the dissolution

The plutonium oxide selected for this study was decomposed plutonium oxalate with >95% of the material having a particle diameter <70 μm as determined by a scanning laser microscopy technique. Attempts to dry sieve the oxide into narrow size fractions prior to dissolution in the HCl-Fe(II) solvent system failed, apparently due to significant interparticle attractive forces. Although sieve splits were obtained, subsequent scanning laser microscopy analysis of the sieve fractions indicated that particle segregation was not accomplished and the individual sieve fractions retained a particle size distribution very similar to the original powder assemblage. This phenomena was confirmed through subsequent dissolution experiments on the various screen fractions which illustrated no difference in kinetic behavior between the original oxide assemblage and the sieve fractions.

Irrespective of the inability to sieve the oxide, the plutonium oxide was found to obey the classic surface reaction controlled nonporous shrinking sphere model. Arrhenius analysis of the dissolution rate data confirmed this observation and indicated an apparent activation energy for the dissolution reaction of 76.6±2.2 kJ/mol over the temperature range 28°C to 65°C, which compared favorably with previously reported values of 54 kJ/mol and 65 kJ/mol.

1 INTRODUCTION

From the recovery of plutonium associated with irradiated reactor fuel to the stabilization of legacy plutonium residues remaining from nuclear weapons production efforts, the dissolution of plutonium oxide prior to separation and purification has proven to be one of the most challenging operational problems within the entire plutonium processing sequence. From the days of the Manhattan Project to the present process flowsheet, the solvent of choice for plutonium oxide dissolution has been boiling, concentrated nitric acid containing fluoride ion. Of all of the metallic oxides capable of producing relatively concentrated solutions in acidic media, plutonium oxide has proven to be the most difficult to dissolve. Ryan and Bray (1980) were among the first to demonstrate that in low acidities (<5 *M*), plutonium oxide is practically insoluble from a thermodynamic basis. The standard free energy of the dissolution reaction in non-complexing acidic media was calculated at 41 kJ/mol, and at the boiling point was only a slightly more favorable -10.5 kJ/mol.

Improvements to the HNO_3-HF system have been suggested that replace the fluoride ion with either strong oxidants like Ce(IV) or Ag(II), or strong reductants such as Cr(II), V(II), U(III) to accomplish solubilization of the plutonium as either Pu(VI) in oxidizing dissolution or as Pu(III) in reducing dissolution. In some cases, these reagents offer significant advantages over

the conventional system, but in general, concerns about adverse impacts on downstream processing operations and current environmental regulatory guidelines definitely preclude the widespread use of many of these proposed alternatives in the United States.

1.1 Purpose of the Research

The attention given to the dissolution of PuO_2 over the past several decades by numerous researchers has been followed closely in hopes that new developments in this area would improve the overall efficiency of oxide dissolution from the wide variety of feed sources that require treatment. The recent detailed oxidative and reductive dissolution studies of Berger (1990) and Machuron-Mandard (1991) are summarized by Madic (1992), and are excellent works describing the introduction and use of electrochemistry in facilitating new approaches to PuO_2 dissolution.

Because there are a variety of matrices contaminated with chloride requiring treatment to separate and recover plutonium, there would be advantages for developing a PuO_2 dissolution technique in a chloride solvent rather than being concerned about matrix compatibility in a nitric acid system. This present study extended prior work by Shakila et al. (1989) and investigated a reductive dissolution technique for plutonium oxide using

Fe(II) in hydrochloric acid. The overall reaction describing PuO_2 dissolution in this solvent system was determined by Shakila as :

$$PuO_2 + 4H^+ + Fe^{+2}_{(aq)} \rightarrow Pu^{+3}_{(aq)} + 2H_2O + Fe^{+3}_{(aq)} \qquad (1.1)$$

In the work by Shakila, reductive dissolution continued so long as ferrous ion was present in solution. They were successful in extending the dissolution reaction by adding a reducing agent to the system, such as hydrazine, to reduce the reaction product Fe(III) to Fe(II) for continued participation in dissolution.

This study extended Shakila's observations to include continuous regeneration of the Fe(II) electron transfer catalyst by bulk electrolysis and the use of cyclic voltammetry as an *in-situ* analytical technique for measuring the progress of the dissolution reaction. An attempt was made to dry-sieve the oxide into fairly narrow particle size ranges to investigate fundamental heterogeneous reaction kinetics, and to determine the best heterogeneous reaction model describing oxide dissolution. Dry-sieving the PuO_2 used in this study failed, due to significant interparticle attractive forces. This did not, however, preclude determining that the classic surface reaction controlled nonporous shrinking sphere model very adequately and appropriately described the dissolution behavior of this system. In addition, the activation

energy of the dissolution reaction was determined by the traditional Arrhenius model and compared favorably to work completed by other investigators.

1.2 Research Goals

The goal of this research was to study the dissolution phenomena of plutonium oxide in the non-traditional HCl-Fe(II) system, and to suggest a heterogeneous model best describing the fluid-solid reaction. In addition to this overall objective, supporting work in this area included:

- evaluating bulk electrolysis for continuous regeneration of the Fe(II) electron transfer catalyst used in this reaction,
- evaluating the effectiveness of cyclic voltammetry as an *in-situ* analytical tool for monitoring the progress of the dissolution reaction,
- evaluating the fundamental nature of heterogeneous PuO_2 dissolution kinetics in this solvent system,
- presenting a general dissolution model for this particle assemblage,
- presenting an estimate of the activation energy of the dissolution reaction as obtained from analysis of the classical Arrhenius model, and

- investigating dry sieving as a method for segregating the PuO_2 assemblage into narrow size fractions for further evaluation.

2 LITERATURE REVIEW

2.1 The Plutonium-Oxygen System

The plutonium-oxygen system has previously been studied in great detail from the view of reactor fuel technology and solid state chemistry. An exhaustive presentation of this information is not necessary to meet the objective of this research, but discussion of some of the basic properties of plutonium oxide is appropriate.

With the exception of PuO, which has not been found to occur as a solid equilibrium phase, there are four plutonium-oxygen phases that have been clearly identified to date. The crystal structure and preparatory techniques of all oxides identified as separate entities are succinctly presented in Katz, Seaborg, and Morss (1986). Two of the phases correspond to stoichiometric compounds represented by $PuO_{2.00}$ (stoichiometric plutonium oxide) and $PuO_{1.50}$ (the β-Pu_2O_3 stoichiometric plutonium sesquioxide phase). The nonstoichiometric phases correspond to two hyperstoichiometric sesquioxides of the forms $PuO_{1.51}$ (α-Pu_2O_3) and $PuO_{1.61}$ (α'-Pu_2O_3); and to the substoichiometric dioxide PuO_{2-X} which extends from $PuO_{1.61}$ to $PuO_{1.98}$ depending on the oxide treatment temperature and the oxygen partial pressure. This material is closely related to $PuO_{2.00}$ but belongs in a different phase region.

Because of handling difficulties, the defect structure and nonstoichiometry of the plutonium oxides has not been studied extensively. The phase diagram of the plutonium-oxygen system as shown in Figure 2.1a is the version originally reported by Ellinger (1968) as a composite presentation of several authors. To date, the entire phase diagram is not well-established, and future work will no doubtably lead to clarifications of the tentatively proposed diagram indicated in Figure 2.1b (Naito et al. 1992).

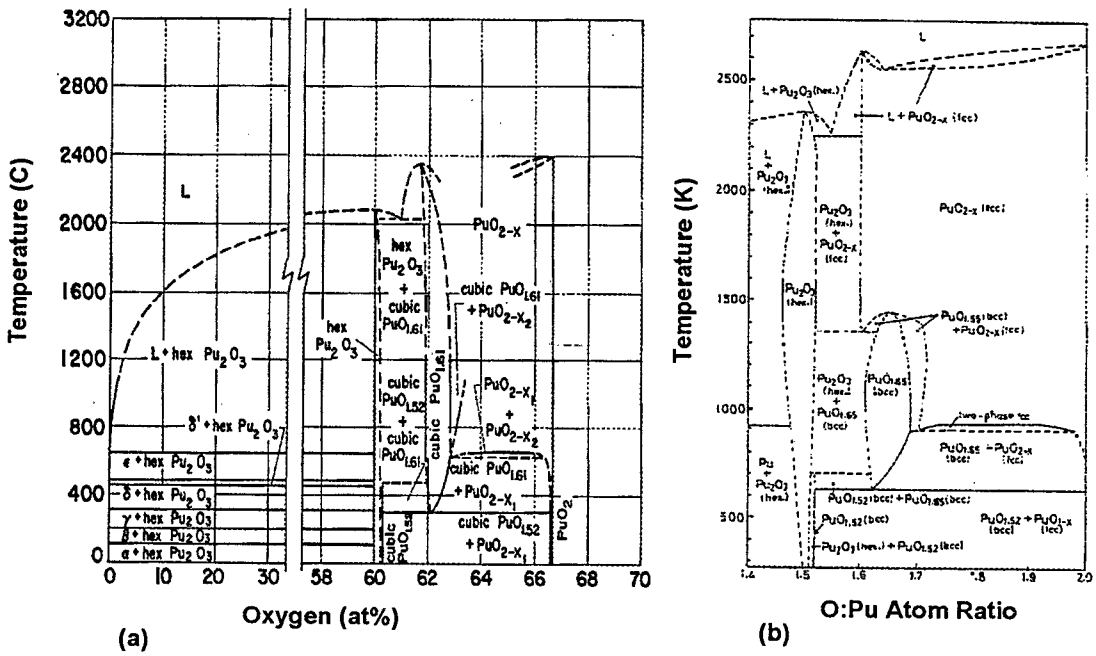

Figure 2.1. Plutonium-oxygen phase diagram; (a) from Ellinger 1968 and (b) from Naito et al. 1992 (Fig. 2.1b reprinted by permission from the American Chemical Society).

2.2 Dissolution of Plutonium Oxide

Numerous researchers have investigated the dissolution of plutonium oxide in aqueous acidic media. As discussed in Benedict, Pigford, and Levi (1981), this step is fundamentally important to the many hydrometallurgical unit operations developed for the nuclear industry. Much of the original research into understanding and improving PuO_2 dissolution has principally been directed towards empirical kinetic studies. Bjorklund and Staritzky (1954), and Gilman (1965, 1968) looked at the pretreatment and subsequent dissolution of PuO_2 under a variety of conditions including dissolution in mineral acids, after fusion, after halogenation, and in the presence of complexing agents. Nitric-hydrofluoric acid has been recognized as the classical industrial plutonium oxide dissolution process with only limited investigations into the alternative hydrochloric acid system (Molen 1967, Crossley and Milner 1969, Bray et al. 1986, Shakila et al. 1989).

Uriarte and Rainey (1965) looked at the dissolution behavior of UO_2, PuO_2 and mixed UO_2-PuO_2 in nitric acid with and without redox or complexing reagents. Other basic studies have also been conducted evaluating the importance of fluoride to successful dissolution (Barney 1976, Tallent and Mailen 1977a, 1977b), while others studied thoria dissolution in hopes it would lead to a better understanding of the plutonia dissolution phenomena (Shying et al. 1970, 1972). Some researchers studied the effect of various

promoters in combination with fluoride to improve dissolution performance (Uriarte and Rainey 1965, Harmon 1975a, 1975b). An electrolytic dissolution procedure using electron transfer catalysts was developed for rapid and complete oxide dissolution in nitric acid systems (Bray and Ryan 1982, Wheelwright et al. 1988, Berger 1992, Ryan et al. 1992).

Ryan and Bray (1980), in their historical review of PuO_2 dissolution, were the first to attempt explain, from a thermodynamic viewpoint, the relative insolubility of plutonium oxide in noncomplexing acid media by calculating the free energy of reaction. In low acidities (<5 *M*), they calculated the standard free energy of the dissolution reaction to be ΔG^0_{298} = 41 kJ/mol, and at the acid boiling point to be only slightly more favorable at ΔG_{373} = -10.5 kJ/mol. As part of a study to systematically evaluate the dissolution behavior of several different actinide oxides, Berger (1990) utilized carbon paste electrochemical techniques and considered the following general dissolution mechanisms for PuO_2:

- with no redox reaction, producing the Pu(IV) species in solution,
- by oxidation, producing either Pu(V) or Pu(VI), and
- by reduction, producing Pu(III).

From Berger (1990) and Madic (1992), only the reductive dissolution path appears thermodynamically favorable in noncomplexing acidic media

(Table 2.1); although oxidation leading to Pu(V) and Pu(VI) can be theoretically observed for electrochemical electrode potentials higher than 1.43 V and 1.22 V respectively, vs. the normal hydrogen electrode (NHE). It should be noted, however, that all of these plutonium redox products have been previously produced by chemical or electrochemical methods.

Table 2.1: Thermodynamic Data for the Dissolution of PuO_2, (Berger 1990)

Reaction	ΔG^0_{298} (kJ/mol)
$PuO_2(s) \rightarrow Pu^{+4}(aq)$	32.4 (±4.00)
$PuO_2(s) \rightarrow Pu^{+3}(aq)$	-64.96 (±4.00)
$PuO_2(s) \rightarrow PuO_2^{+}(aq)$	138.27 (±9.79)
$PuO_2(s) \rightarrow PuO_2^{+2}(aq)$	236.19 (±15.40)

In spite of the pessimistic thermodynamic data presented in Table 2.1, dissolution of PuO_2 is practiced on a daily basis using fluoride complexation equilibria to shift the thermodynamics presented in Table 2.1 into a favorable region and achieving effective solubilization of Pu(IV).

2.2.1 PuO_2 Dissolution Without Redox

Numerous acid media have been recommended for the dissolution of PuO_2 without changing the plutonium valance state. As described in Crossley and Milner (1969), Dahlby et al. (1975), and Machuron-Mandard (1991), these procedures have been limited to the analytical field and generally require extreme physicochemical conditions to achieve effective dissolution of the PuO_2 (concentrated HCl and HNO_3 at 100°C to 300°C and pressures as high as 4000 psig; concentrated HCl and $HClO_4$ or H_2SO_4 at 300°C; or H_3PO_4 at 200°C).

From Ryan and Bray (1980), nitrate ion in solution leads to the complexing equilibria of Pu(IV); and in the presence of high concentrations of nitric acid, the Pu(IV) complexation is sufficient to produce moderately favorable thermodynamics for the overall PuO_2 dissolution reaction. Considering only Pu(IV) and $Pu(NO_3)^{+3}$ as soluble species, they calculated the solubility of PuO_2 at 100°C (Figure 2.2). The solubility limits reported for high nitric acid concentrations are lower than real values, however, since plutonium nitrate complexes with higher valence states of plutonium were not considered in the theoretical presentation.

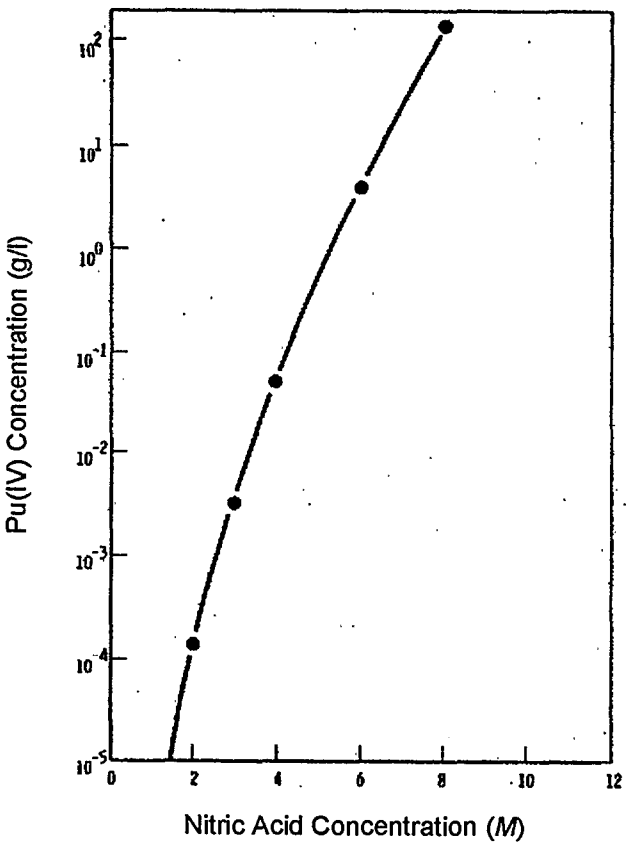

Figure 2.2. Theoretical solubility of PuO_2 in nitric acid (Ryan and Bray 1980; reprinted by permission from the American Chemical Society).

The majority of studies on the dissolution of PuO_2 in nitric-hydrofluoric acid did not include detailed thermodynamic analysis; and only elaborated on the beneficial role played by the fluoride ion. Besides its strong ability to form highly stable complexes with Pu(IV), evidently enhancing the dissolution thermodynamics, fluoride ion was also thought to promote a fundamentally different oxide surface reaction mechanism than the one observed in pure

nitric acid, thereby causing increased reaction kinetics. Work on describing the interaction of fluoride with the plutonium oxide during nitric-hydrofluoric acid dissolution was completed by Barney (1976) and Tallent (1977a).

2.2.2 Oxidative PuO_2 Dissolution

In an attempt to improve PuO_2 dissolution kinetics and move away from the aggressive nature of the boiling nitric-hydrofluoric acid solvent, industrial improvements led to the implementation of redox chemistry. Wilson (1961) and later Uriarte and Rainey (1965) and Harmon (1975a and 1975b), investigated the use of Ce(IV) as a promoter to enhance the performance of the nitric-hydrofluoric acid process. This reagent was successful because the Ce(IV)-Ce(III) half-cell potential (1.61 V vs. NHE in 1.0 *F* HNO_3) was higher than the potential required to oxidize Pu(IV) to either Pu(V) or Pu(VI). These values were determined by Berger (1990) to be 1.43 V and 1.22 V vs. NHE, respectively.

Other oxidative reagents have been evaluated for PuO_2 dissolution or the destruction of plutonium-contaminated organic materials using the Ag(II)-Ag(I) couple (1.929 V vs. NHE in 4 *F* HNO_3) reported by Berger (1990), Ryan et al. (1992), and Zawodzinski et al. (1993); and the Co(III)-Co(II) couple (1.85 V vs. NHE in 4 *F* HNO_3) reported by Zawodzinski (1996). CEPOD, as discussed by Ryan et al. (1992), is an acronym for Catalyzed

Electrochemical Plutonium Oxide Dissolution and was developed to dissolve PuO_2 by oxidizing Pu(IV) from the oxide crystal lattice to form the more soluble PuO_2^{+2}. Successful CEPOD solvents contain catalytic amounts of elements that form kinetically fast, strongly oxidizing ions that can be continuously regenerated at an electrochemical anode. In their oxidized form, the catalysts offering the most promise include Ag(II), Ce(IV), Co(III), and AmO_2^{+2}.

2.2.3 Reductive PuO_2 Dissolution

An early example of reductive dissolution was found in Bjorklund and Staritzky (1954), where they observed the rapid dissolution of PuO_2 in a mixture of hydrochloric acid and potassium iodide. Until recently, other studies involving reductive dissolution have been practically nonexistent. Berger (1990) estimated the standard potential of the $PuO_2(s)/Pu^{+3}(aq)$ couple to be +0.67 V vs. NHE; and Machuron-Mandard (1991), extended this work to examine the reductive dissolution of PuO_2 using the Cr(II)/Cr(III) couple in sulfuric acid media (-0.42 V vs. NHE). Shakila et al. (1989) examined the reductive dissolution of PuO_2 in hydrochloric media using ferrous ion as an electron transfer catalyst. Although the Fe(II)/Fe(III) couple is reported as 0.732 V vs. NHE in 1 *F* HCl, it was found to be approximately 0.55 V vs. NHE in 7 *M* HCl (according to anodic peak height measurements

from the cyclic voltammograms generated in this present study). In Shakila's work, the oxide dissolution reaction proceeded vigorously as long as Fe(II) was present in solution. They also observed that the use of a reducing agent (hydrazine) in conjunction with Fe(II) prolonged the dissolution rate supposedly due to reduction of the Fe(III) product back to the Fe(II) reactant thereby continuing the reduction of Pu(IV) to the more soluble Pu(III). In an earlier investigation, Shakila et al. (1987) also observed that hydrazine led to improved PuO_2 dissolution in the HNO_3-HF system.

2.3 Heterogeneous Reaction Systems

2.3.1 PuO_2 Dissolution Kinetics

Although several basic studies have been conducted attempting to evaluate the dissolution kinetics of PuO_2 in HNO_3-HF, the principle conclusion from the past work was that very little agreement among the various researchers existed regarding the effect of various parameters on the dissolution rate. There was certain agreement that oxide surface area, fluoride concentration, nitric acid concentration, and solvent-to-oxide ratio were of primary importance at a given temperature (usually 100°C). It was also generally concluded that as the PuO_2 dissolution proceeded, the rate

decreased as free fluoride was complexed with Pu(IV) or consumed by other parasitic side reactions. As discussed previously, Ryan and Bray (1979), presented a fairly comprehensive review of plutonium dioxide dissolution in the nitric acid system using fluoride ion in conjunction with several reaction promoters.

Uriarte (1965) found the dissolution rate of PuO_2 to increase by the 1.4^{th} power of HF molarity at constant acidity and by the 4^{th} power of the total HNO_3 molarity. Barney (1976) found the rate to be first order in the total HF not complexed by Pu(IV); first order in oxide surface area, and independent of acid concentration in the range 4 *M* to 12 *M*. He also found the dissolution rate to decrease with the amount of PuO_2 dissolved because fluoride was complexed with Pu(IV) in solution. This effect increased with decreasing acidity due to the formation of higher fluoro complexes at lower acidities. Tallent and Mailen (1977a, 1977b) also found the rate to be first order in uncomplexed HF concentration and found the rate to be first order in mean ionic activity of HNO_3 (second order if fluoride ion instead of HF was the reacting species). They also recognized that the rate decreased as the fluoride was complexed by Pu(IV) and performed experiments to eliminate this effect by oxidizing the Pu(IV) to Pu(VI), which forms a much weaker fluoro complex.

Despite the rather wide differences in conclusions with regard to the effect of acidity on dissolution rate, the values of the *initial* rate from these studies were in rather good agreement for dissolution in 8 *M* to 10 *M* HNO_3-0.05 *M* HF at 100°C; all in the range of $1 \cdot 10^{-3}$ to $9 \cdot 10^{-3}$ mg PuO_2 min^{-1}-cm^{-2}. Tallent and Mailen (1977a) indicated that the dissolution of PuO_2 followed a mechanism similar to a thoria dissolution mechanism proposed by Shying et al. (1972), and that the rate controlling step for PuO_2 dissolution involved the reaction of protons and fluoride ions with the fluorinated PuO_2 surface sites.

$$PuOF + F^- + 2H^+ \rightarrow PuF_2^{+2} + H_2O + e^- \qquad (2.1)$$

Tallent and Mailen (1977a) suggested that if PuO_2 dissolution followed the thoria dissolution mechanism proposed by Shying et al. (1972), the PuF_2^{+2} complex would dissociate in solution and the electron would re-adsorb or react with the remaining PuO_2 surface sites as the first step in continued dissolution.

Considering the dissolution of thoria in HNO_3-HF (which is chemically similar to PuO_2); Takeuchi et al. (1971) found the dissolution rate of the ThO_2 to be less than first order in HF concentration and proportional to

$$\frac{K_1[HF]}{1 + K_1[HF]} \qquad (2.2)$$

where K_1 was determined empirically.

This observation was found to be accurate in the HF concentration range 0.01 *M* to 0.05 *M* where ThO_2 dissolution was found to be first order in uncomplexed HF concentration. Takeuchi also found a small dependence on total acidity of the same form

$$\frac{K_2[HNO_3]}{1+K_2[HNO_3]} \tag{2.3}$$

where K_2 was also determined empirically.

Barney (1976) had previously found a similar result for the dissolution of PuO_2.

In severe contrast to the work completed in the nitric acid system, there has been relatively little attention paid to other solvent systems. Molen (1967) compared the dissolution behavior of PuO_2 in HNO_3-CaF_2 to the dissolution of PuO_2 in the HCl-$SnCl_2$ system and found generally a better performance by the HCl solvent. His work was semi-quantitative, however, and illustrated oxide dissolution behavior graphically as a function of particle surface area, solid-to-liquid ratio, and mean crystallite size.

Bray et al. (1986) extended work from the nitric acid system to the HCl system and included mixtures of HCl-CaF_2 where they also found that the dissolution rate of the oxide decreased markedly as the calcination temperature of the oxide increased. They also, however, observed acceptable dissolution performance in boiling HCl that contained varying

molar ratios of fluoride-to-plutonium. Oxide fired to ~1700°C was essentially completely dissolved in 3 hours with a fluoride-to-plutonium molar ratio of 2; whereas oxide fired to only 950°C was completely dissolved in ~1 hour at a fluoride-to-plutonium molar ratio of 1.8.

As previously discussed, there has been a remarkable lack of research into reductive PuO_2 dissolution with the exception of work by Shakila et al. (1989) who looked at the dissolution of plutonium oxide in the presence and absence of reducing agents at solution temperatures of ~100°C; and recent work by Machuron-Mandard (1991), where the reductive dissolution of PuO_2 was studied in a dilute solution of H_2SO_4-Cr(II) at 55°C to 65°C.

Shakila's results indicated that the addition of hydrazine increased the dissolution of oxide even at low acidities, and the presence of low concentrations of Fe(II) were sufficient to complete PuO_2 dissolution in approximately 2 hours. Their work showed that dissolution appeared to stop when all of the Fe(II) was converted to Fe(III) and also showed the reaction could be extended by using hydrazine to convert the iron back to the +2 oxidation state. As a result of their study, they proposed the following overall dissolution reaction for the HCl-Fe(II) system as presented previously:

$$PuO_2 + 4H^+ + Fe^{+2}_{(aq)} \rightarrow Pu^{+3}_{(aq)} + 2H_2O + Fe^{+3}_{(aq)} \qquad (1.1)$$

Similarly, Machuron-Mandard examined the reductive dissolution of PuO_2 in the H_2SO_4-Cr(II) system. As with iron in Shakila's research, the chromium electron transfer catalyst was added in the reduced state and allowed to spontaneously reduce plutonium according to the following reaction:

$$PuO_2 + 4H^+ + Cr^{+2}_{(aq)} \rightarrow Pu^{+3}_{(aq)} + 2H_2O + Cr^{+3}_{(aq)} \quad (2.4)$$

Machuron-Mandard, however, did evaluate the effect of agitation, Cr(II) concentration, PuO_2 surface area, temperature, and proton concentration on the overall dissolution rate. He concluded the empirical rate law for dissolution in the H_2SO_4-Cr(II) system took the form:

$$v = 1.8 \cdot 10^4 \cdot S \cdot \exp\left[\frac{(-6.5 \pm 5) \cdot 10^3}{RT}\right] \cdot \left[H^+\right]^{(0.4 \pm 0.1)} \quad (2.5)$$

where:

v is the dissolution rate (mol PuO_2/sec),

S is the BET (Brunauer, Emmett, and Teller) surface area (m^2/g),

R is the gas constant (8.314 j/mol-K),

T is the absolute temperature (K), and

$\left[H^+\right]$ is the proton concentration (M).

2.3.2 Noncatalytic Fluid-Solid Reactions

The majority of models for fluid-solid reactions were originally developed based on the simplifying assumption of a nonporous reactant, even when the reactant was known to contain considerable porosity. This simplification may confound data interpretation, but it is generally the approach taken by many researchers when studying a new reaction system. An important characteristic of nonporous solid reactions is that chemical reaction and mass transport are coupled in series. Since the chemical reaction occurs at the planar surface of the solid, the surface always appears as one of the boundary conditions in the mass transport equations. This makes analysis of the nonporous solid systems easier than the analysis of porous solid systems.

The simplest system in fluid-solid reactions is that of a shrinking nonporous particle that forms no solid product layer:

$$aA_{fluid} + bB_{solid} \rightarrow cC_{fluid} \tag{2.6}$$

Figure 2.3 illustrates the reaction schematically.

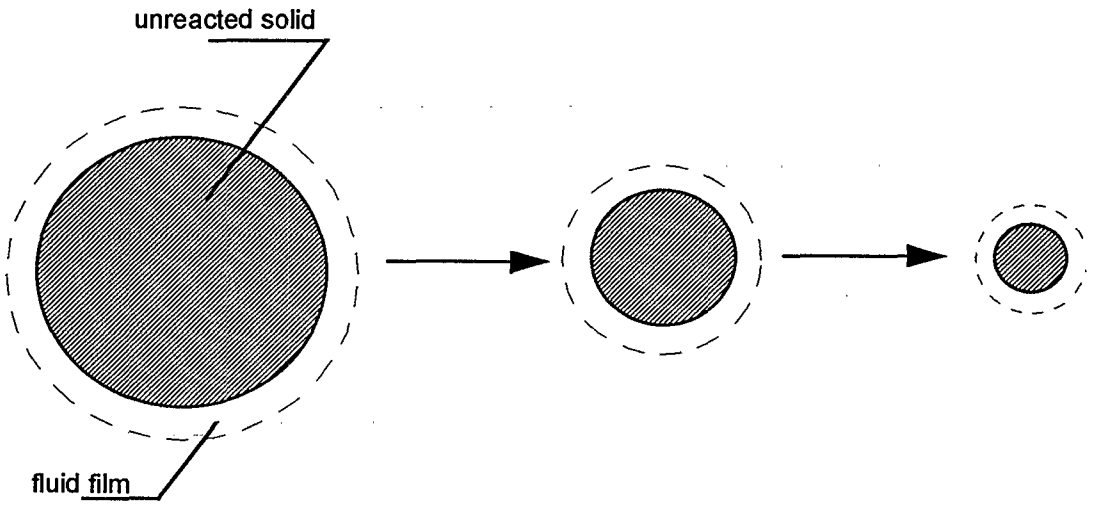

Figure 2.3. Representation of a nonporous solid reacting with a fluid in which no solid product is formed.

In many situations, these nonporous fluid-solid interactions are accurately approximated by first-order reactions. The rate expression obtained for the reaction is determined from the rate limiting step based on the sequence of actions found in Table 2.2 and generally takes a form similar to

$$\frac{dA}{dt} = k[C_A^n - (C_C^m / K_E)] \tag{2.7}$$

where $\frac{dA}{dt}$ is the disappearance of A by surface chemical reaction,

k is the heterogeneous rate constant,

C_A and C_C are the fluid reactant and product concentrations, respectively, at the reaction surface, and

K_E is the equilibrium constant.

When the reaction orders $n = m = 1$, and the reaction is irreversible (as most fluid-solid reactions are), the rate becomes first order. This, in addition to its mathematical simplicity, is why first order kinetics are frequently used for describing many types of fluid-solid reactions.

Table 2.2. Rate-Limiting Mechanisms for Nonporous Fluid-Solid Reactions

Progressive Step	Rate-Limiting Mechanism
1	Diffusion of the fluid reactants across the fluid film surrounding the solid.
2	Adsorption of the fluid reactants at the solid reactant surface.
3	Chemical reaction with the solid surface.
4	Desorption of the fluid products from the solid reaction surface.
5	Diffusion of the fluid products away through the fluid film surrounding the solid.

Development of the following general models considers both porous and nonporous fluid-solid reactions and are some examples of the variety and complexity of models available for examining reaction systems in this area. These examples consider isothermal systems of spherical particles reacting with first order kinetics at quasi-steady state to produce only fluid products.

2.3.2.1 Nonporous Shrinking Spherical Particle–Surface Chemical Reaction Control

For a nonporous (large) shrinking spherical particle under chemical reaction control, the conversion-time relationship originally given by Wen (1968) and Levenspiel (1972) is:

$$\frac{t}{\tau_{rxn}} = 1-(1-X)^{1/3} \tag{2.8}$$

where $\tau_{rxn} = \frac{\rho_B R}{b k_s C_{Af}}$ = time for complete particle conversion

ρ_B = molar density of species B in the solid material (mol/cm^3),

R = initial particle radius (cm),

b = stoichiometric ratio (moles of solid reacted per mole of fluid reactant),

k_s = first order rate constant for the surface reaction (cm/sec),

C_{Af} = bulk solution concentration of species A (mol/cm^3), and

X = fractional particle conversion (dimensionless).

This result can be developed assuming that the following general reaction describes the dissolution process:

$$aA_{fluid} + bB_{solid} \rightarrow cC_{fluid} \tag{2.6}$$

The amount of B_{solid} present in a sphere of radius R is

$$N_B = \rho_B V = \rho_B \tfrac{4}{3}\pi R^3 \tag{2.9}$$

where ρ_B = molar density of species B (mole/cm^3),

R = the initial radius of the unreacted core (cm), and

V = the volume of the sphere containing species B (cm^3).

As dN_B moles of solid reactant disappear, the decrease in volume or radius of the unreacted core is given by

$$-dN_B = -bdN_A = -\rho_B dV = -\rho_B d(\tfrac{4}{3}\pi r^3) = -4\pi\rho_B r^2 dr \tag{2.10}$$

where r is the radius of the unreacted core at any time.

The decrease in solid reactant B is controlled by the rate of surface chemical reaction and is proportional to the available surface area of the reacting particle. In this reaction, film diffusion is fast compared to the surface reaction, thus, dN_B is dependent on the available surface of the unreacted particle, and the a rate of reaction is given by

$$-\frac{1}{4\pi r^2}\frac{dN_B}{dt} = -\frac{b}{4\pi r^2}\frac{dN_A}{dt} = bk_s C_{Af} \tag{2.11}$$

And by combining Eq. 2.10 and 2.11, the rate of reaction in terms of the shrinking particle radius can be written as

$$-\frac{1}{4\pi r^2}(4\pi\rho_B r^2)\frac{dr}{dt} = bk_s C_{Af} = -\rho_B \frac{dr}{dt} \tag{2.12}$$

integrating

$$-\rho_B \int_R^r dr = bk_s C_{Af} \int_o^t dt \tag{2.13}$$

$$t = \frac{\rho_B}{bk_s C_{Af}}(R - r) \tag{2.14}$$

At $r = 0$, the reaction is complete; therefore, the time for complete reaction τ_{rxn}, is given by

$$\tau_{rxn} = \frac{\rho_B R}{bk_s C_{Af}} \tag{2.15}$$

and

$$\frac{t}{\tau_{rxn}} = 1 - \frac{r}{R} \tag{2.16}$$

Since the fractional conversion X is given by the volume change in the particle

$$X = \frac{\frac{4}{3}\pi R^3 - \frac{4}{3}\pi r^3}{\frac{4}{3}\pi R^3} = 1 - \frac{r^3}{R^3} \tag{2.17}$$

or

$$\frac{r}{R} = (1 - X)^{1/3} \tag{2.18}$$

Therefore, the general form of the relationship for a nonporous shrinking spherical particle governed by surface chemical reaction results in Eq. 2.8.

$$\frac{t}{\tau_{rxn}} = 1 - (1 - X)^{1/3} \tag{2.8}$$

2.3.2.2 Nonporous Shrinking Spherical Particle–Diffusion Control for Small Particles in the Stokes' Law Regime

For a nonporous (small) shrinking spherical particle in the Stokes' law regime, the fluid dynamics of the system are quiescent and laminar with a Reynolds number less than one. In this case, the experimental drag force for a sphere is the same as the theoretical Stokes' law equation. Essentially this fluid-solid system is unmixed and film diffusion controls the reaction. For this system, the conversion-time relationship becomes (Levenspiel 1972):

$$\frac{t}{\tau_{spf}} = 1-(1-X)^{2/3} \tag{2.19}$$

where $\tau_{spf} = \frac{\rho_B R^2}{2bC_{Af}D_e}$ = time for complete particle conversion

D_e = effective diffusivity in the fluid film surrounding the particle (cm^2/sec) and definitions for the other parameters are given in section 2.3.2.1.

Levenspiel (1972) illustrates the development of this relationship from previously correlated mass transfer relationships. Film resistance to mass transfer at a particle surface will be dependent on many factors; fluid and particle velocity, particle size, and various fluid properties. An example of an applicable mass transport correlation for a component of mole fraction y in a fluid to free-falling solids is given by Ranz and Marshall (1952)

$$\frac{k_g d_p}{D_e} = 2 + 0.6(Sc)^{1/3}(\mathrm{Re})^{1/2} = 2 + 0.6\left(\frac{\mu}{\rho D_e}\right)^{1/3}\left(\frac{d_p \rho u}{\mu}\right)^{1/2} \tag{2.20}$$

where

k_g = fluid phase mass transfer coefficient (cm/sec),

d_p = particle diameter (cm),

Sc = Schmidt number = $\frac{\mu}{\rho D_e}$ (dimensionless),

Re = Reynolds number = $\frac{d_p \rho u}{\mu}$ (dimensionless),

ρ = mass density (g/cm^3),

μ = fluid viscosity (g/cm sec), and

u = fluid velocity (cm/sec).

At the time when a nonporous spherical particle originally of radius R has reacted and shrunk to size r, the molar flux of the solid reactant is

$$dN_B = \rho_B dV = 4\pi\rho_B r^2 dr \tag{2.21}$$

Analogous to the surface reaction control development (Eq. 2.11), the amount of material reacting is proportional to the available surface of the unreacted particle. Since fluid film diffusion controls the reaction, the gradient of the fluid reactant concentration between the bulk fluid phase and the particle surface is the driving force for the reaction. This can be further simplified recognizing that the reactant concentration at the particle surface

is zero due to the speed of the surface reaction relative to mass transfer ($k_s >> k_g$). Combining Eq. 2.21 with the mass transfer analog to Eq. 2.11 results in

$$-\frac{1}{4\pi r^2}\frac{dN_B}{dt} = -\frac{\rho_B 4\pi r^2}{4\pi r^2}\frac{dr}{dt} = -\rho_B \frac{dr}{dt} = bk_g(C_{Af} - C_{As}) = bk_g C_{Af} \qquad (2.22)$$

where C_{As} is the fluid reactant concentration at the particle surface.

For a fluid-particle reaction taking place in the Stokes' law regime, the fluid velocity and the particle diameter are sufficiently small and Eq. 2.20 reduces to

$$k_g = \frac{2D_e}{d_p} = \frac{D_e}{r} \qquad (2.23)$$

Combining Eq. 2.22 and 2.23 and integrating produces

$$-\rho_B \frac{dr}{dt} = \frac{bD_e C_{Af}}{r} \Rightarrow -\int_R^r r dr = \frac{bD_e C_{Af}}{\rho_B}\int_0^t dt \qquad (2.24)$$

and

$$\frac{R^2 - r^2}{2} = \frac{bD_e C_{Af} t}{\rho_B} \qquad (2.25)$$

At $r = 0$, $t = \tau_{spf}$; the time for complete disappearance of the particle

$$\tau_{spf} = \frac{\rho_B R^2}{2bD_e C_{Af}} \qquad (2.26)$$

Therefore

$$\frac{t}{\tau_{spf}} = 1 - \left(\frac{r}{R}\right)^2 \tag{2.27}$$

And employing Eq. 2.18 resulted in the time-conversion relationship

$$\frac{t}{\tau_{spf}} = 1 - (1 - X)^{2/3} \tag{2.19}$$

2.3.2.3 Nonporous Shrinking Spherical Particle–Diffusion Control for Large Particles with Initially High Reynolds Number

In a system where the fluid dynamics produce initially a high Reynolds number around a large, nonporous, shrinking spherical particle controlled by film diffusion, the conversion-time relationship previously given by Levenspiel (1972) is:

$$\frac{t}{\tau_{lpf}} = 1 - (1 - X)^{1/2} \tag{2.28}$$

where $\tau_{lpf} = \dfrac{(const)R^{3/2}}{C_{Af}}$ = time for complete particle conversion.

Development of this diffusion control model is similar to the model developed for diffusion control in the Stokes' law regime. In the Stokes' law regime

$$k_g \propto \frac{1}{d_p} \qquad \text{for small } d_p \text{ and } u \tag{2.29}$$

while for larger particles with an initially high Reynolds number

$$k_g \propto \frac{u^{1/2}}{d_p^{1/2}} \qquad \text{for large } d_p \text{ and } u \tag{2.30}$$

For this situation

$$k_g = \frac{const}{d_p^{1/2}} = \frac{const}{r^{1/2}} \tag{2.31}$$

The constant in Eq. 2.31 can be evaluated from the mass transfer correlation used in the development (Eq. 2.20 for example). At a high Reynolds number, Eq. 2.20 reduces to

$$k_g = \frac{0.6 D_e \left(\frac{\mu}{\rho D_e}\right)^{1/3} \left(\frac{d_p \rho u}{\mu}\right)^{1/2}}{d_p} = \frac{const}{d_p^{1/2}} \tag{2.32}$$

This result can be used in the development of Eq. 2.28, by following a procedure similar to the one previously performed in Section 2.3.2.2,

$$-\rho_B \frac{dr}{dt} = \frac{bC_{Af}(const)}{r^{1/2}} \Rightarrow -\int_R^r r^{1/2} dr = C_{Af}(const)\int_0^t dt \tag{2.33}$$

and

$$R^{3/2} - r^{3/2} = C_{Af}(const)t \tag{2.34}$$

At $r = 0$, $t = \tau_{lpf}$; the time for complete disappearance of the particle

$$\tau_{lpf} = const \frac{R^{3/2}}{C_{Af}} \tag{2.35}$$

Therefore

$$\frac{t}{\tau_{lpf}} = 1 - \left(\frac{r}{R}\right)^{3/2} \tag{2.36}$$

And again employing Eq. 2.18 results in the time-conversion relationship

$$\frac{t}{\tau_{lpf}} = 1 - (1 - X)^{1/2} \tag{2.28}$$

2.3.2.4 Uniformly Reacting Porous Spherical Particle–Surface Chemical Reaction Control

Peterson (1957) and Sohn (1976) studied the involved nature of noncatalytic heterogeneous reactions in an initially porous particle, and although there are several extensions to this general model (Ishida and Wen 1968, 1971, Park and Levenspiel 1975, Szekely et al. 1976), the following is presented only as a representative example of the rigor of some of these heterogeneous fluid-solid models.

For uniformly reacting porous particles where the fluid species can penetrate deeply into the interior of the solid prior to reacting (chemical reaction controlling), the rate of reaction per unit volume is given by (Sohn 1976):

$$R(v) = kC_A^n \left(\frac{\varepsilon_0}{r_0}\right) \frac{(2G - 3\varsigma)\varsigma}{G - 1} \tag{2.37}$$

and the relationship between conversion and time is

$$X = \frac{\varepsilon_0}{1-\varepsilon_0}\left[\left(1+\frac{t}{\tau}\right)^2\left(\frac{G-1-\frac{t}{\tau}}{G-1}\right)-1\right] \tag{2.38}$$

where k = fluid-solid reaction rate constant (cm/sec),

$\varsigma = r/r_0$

ε_0 = initial porosity of the solid (dimensionless),

r_0 = initial radius of pores (cm),

r = pore radius at any time (cm),

C_A = molar concentration of reactant A (mol/cm^3),

$G = 3\pi L / Kr_0$,

L = total length of the pore system per unit volume defined as the centerline distances of the individual pores,

K = characteristic constant depending on the number of pore intersections per unit volume and the angles at which they intersect,

$\tau = \frac{r_0\rho_s}{bkC_A^n}$ = time for complete particle conversion (sec),

ρ_s = molar density of the pore-free solid (moles/cm^3),

b = stoichiometric ratio (moles of solid reacted per mole of fluid reactant), and

n = order of reaction.

For the general reaction described by Eq. 2.6, and governed by chemical reaction control, the rate of reaction per unit volume of porous solid is given by

$$\left(\frac{\rho_s S_v}{b}\right)\frac{dr}{dt} = \frac{\rho_s}{b}\frac{d\varepsilon}{dt} \Rightarrow S_v = \frac{d\varepsilon}{dr} \tag{2.39}$$

where

S_v = surface area to volume ratio of the solid (cm^{-1}), and

ε = porosity of the solid at any time.

and recognizing as well that

$$\frac{dr}{dt} = \frac{bk}{\rho_s} C_A^n \tag{2.40}$$

To solve Eq. 2.39, a relationship for the surface area to volume ratio and the pore radius is necessary. In the original development, Petersen (1957) considers a porous solid represented by an idealized network of cylindrical pores with random intersections; and for a constant concentration of fluid reactant, the cylindrical pore radii increase uniformly from r_0 to r. After geometric considerations and assuming that no new pores are created, the relationship for surface area becomes

$$S_v = 2\pi r L - Kr^2 \tag{2.41}$$

where L is the total length of the pore system per unit volume, and

K is a characteristic constant depending on the number of pore intersections per unit volume and the angles at which the poles intersected each other.

From Eq. 2.39 and Eq. 2.41

$$\varepsilon = \int_0^r (2\pi rL - Kr^2)dr = \pi Lr^2 - \frac{K}{3}r^3 \tag{2.42}$$

When $r = r_0$, $\varepsilon = \varepsilon_0$, therefore

$$\frac{\varepsilon}{\varepsilon_0} = \frac{\pi Lr^2 - (K/3)r^3}{\pi Lr_0^2 - (K/3)r_0^3} = \varsigma^2\left(\frac{G-\varsigma}{G-1}\right) \tag{2.43}$$

As defined earlier, $\varsigma = r/r_0$ and G is determined to be $3\pi L/Kr_0$ by rearranging terms in Eq. 2.43. Recognizing that as $\varepsilon \to 1$, $S_v \to 0$. By combining Eq. 2.39 and 2.43, the surface area relationship S_v becomes

$$S_v = \frac{d\varepsilon}{r_0 d\varsigma} = \frac{\varepsilon_0}{r_0}\frac{(2G-3\varsigma)\varsigma}{G-1} \tag{2.44}$$

For $S_v = 0$ at $\varepsilon = 1$, the term $2G - 3\varsigma = 0$ at $\varepsilon = 1$. Therefore

$$\varsigma\big|_{\varepsilon=1} = \frac{2G}{3} \tag{2.45}$$

Upon combining Eq. 2.45 with Eq. 2.43 results in $G = G(\varepsilon_0)$ only; and can be reduced to

$$\frac{4\varepsilon_0 G^3}{27} - G + 1 = 0 \tag{2.46}$$

And combining Eq. 2.38 with Eq. 2.43 produces

$$kS_v C_A^n = kC_A^n(\frac{\varepsilon_0}{r_0})\frac{(2G-3\varsigma)\varsigma}{G-1} \tag{2.47}$$

which was initially presented as Eq. 2.37.

A relationship between conversion and time can be developed by first integrating Eq. 2.40

$$\frac{dr}{dt} = \frac{bk}{\rho_s}C_A^n \Rightarrow \int_{r_o}^{r} dr = \frac{bkC_A^n}{\rho_s}\int_0^t dt \Rightarrow r - r_0 = \frac{bkC_A^n t}{\rho_s} \Rightarrow \frac{r}{r_0} - 1 = \frac{bkC_A^n t}{r_0\rho_s} \tag{2.48}$$

Since

$$\frac{r}{r_0} = \varsigma = 1 + \frac{t}{\tau} \tag{2.49}$$

where $\tau = \frac{r_0\rho_s}{bkC_A^n}$, the total time for conversion of the porous solid.

Since during the reaction, porosity is developed and continues to increase as the reaction proceeds; the void space in the initial solid ranges from 0 to 1. Conversion of the solid can be described as

$$X = \frac{\varepsilon - \varepsilon_0}{1-\varepsilon_0} \Rightarrow \frac{X(1-\varepsilon_0)}{\varepsilon_0} = \frac{\varepsilon}{\varepsilon_0} - 1 \Rightarrow X = \frac{\varepsilon_0}{1-\varepsilon_0}\left(\frac{\varepsilon}{\varepsilon_0} - 1\right) \tag{2.50}$$

Combining Eq. 2.43 and Eq. 2.49 into the final result of Eq. 2.50 produces the final conversion and time relationship

$$X = \frac{\varepsilon_0}{1-\varepsilon_0}\left[\left(1+\frac{t}{\tau}\right)^2\left(\frac{G-1-\frac{t}{\tau}}{G-1}\right) - 1\right] \tag{2.38}$$

2.3.2.5 Concluding Remarks

In considering these examples of model development, they only begin to illustrate the different levels of simplicity leading to complexity that have been utilized in describing heterogeneous fluid-solid reactions. Wen (1968) supports the philosophy of inspecting simple, but applicable models before developing complex ones.

He qualitatively describes the situation of uncatalyzed heterogeneous fluid-solid reaction controlled by surface chemical reaction control as depending on the rate limiting mechanism selected, the resulting rate equation may involve more than two arbitrary constants, and sometimes as many as seven. In selecting the constants for each mechanism, the curve representing the rate equation is chosen to best fit of the experimental data. But because of intrinsic scatter in the data, however, little meaning can be attributed to many of the constants; and often, the difference in fit between competitive rate expressions is so slight that it can be difficult to determine whether the difference is due to experimental error or due truly to a difference in mechanism.

Although an alternative mechanism may fit the data equally well, the new model may require additional experimentation to confirm the true mechanism. He concluded that although an understanding of the true mechanism would allow for extrapolation beyond the region of investigation;

there are no reasons why simple rate equations fitting the data satisfactorily should not be used provided no extrapolation beyond the original range of investigation is allowed.

2.4 Effect of Temperature on the Rate Determining Step

Generally, for liquid-phase heterogeneous reactions controlled by diffusional processes, the activation energy is low with values ranging between 10 kJ/mol and 20 kJ/mol (Habashi 1969, Terry 1983, Machuron-Mondard 1990). For reactions controlled by chemical reaction at the particle surface, however, values of the apparent activation energy are generally greater than 40 kJ/mol. In liquid solutions, this is due to the linear dependence of the diffusion coefficient with temperature, and can be described by semi-empirical correlations such as the Stoke's-Einstein equation or the Wilke-Chang relationship (Geankoplis 1983). In contrast, the chemical reaction rate constant is exponentially dependent on temperature as illustrated by the Arrhenius relationship.

Stokes-Einstein equation: $$D_{AB} = \frac{9.96 \cdot 10^{-16} T}{\mu V_A^{0.333}} \qquad (2.51)$$

where D_{AB} is the diffusivity of solute A in solvent B (cm^2/sec),

T is the absolute temperature (°K),

μ is the solution viscosity (kg/m·sec), and

V_A is the solute molar volume at its normal boiling point (m^3/kg mol).

Wilke-Chang correlation: $$D_{AB} = 1.173 \cdot 10^{-16} (\varphi M_A)^{0.5} \frac{T}{\mu_B V_A^{0.6}} \qquad (2.52)$$

where φ is an "association parameter" (Geankoplis 1983),

M_B is the molecular weight of the solvent B (kg/kg mol), and

μ_B is the viscosity of the solvent B in (kg/m·sec).

Arrhenius relationship: $$k = k_0 e^{-E_a/RT} \qquad (2.53)$$

where k is a general n^{th}-order heterogeneous rate constant ($(mol/cm^3)^{1-n} \cdot sec^{-1}$),

k_0 is the pre-exponential factor (cm/sec),

E_a is the apparent activation energy (J/mol),

R is the gas constant (8.314 J/mol·K), and

T is the absolute temperature (°K).

For reactions in aqueous solutions, therefore, a doubling of the *absolute* temperature nearly doubles the diffusivity, but the chemical reaction

rate constant can be increased by two orders of magnitude or more depending on the activation energy of the system. For this reason, the activation energy of diffusion controlled processes is characterized as being 10 kJ/mol to 20 kJ/mol while chemical reaction controlled processes usually exhibit activation energies greater than 40 kJ/mol.

This generality, however, is limited to reactions in aqueous solution and some gas-phase systems, and may not apply to catalytic reactions or other systems where strong interparticle pore diffusion or external mass transfer resistances dominate (Smith 1970, Levenspiel 1972, Szekely et al. 1976, Sohn and Wadsworth 1979, Froment and Bischoff 1990, Fogler 1992). In these situations, falsification of the kinetic rate coefficients and the activation energy can occur due to diffusion effects. The magnitude of the effect of this falsification can be illustrated by applying an Arrhenius-type temperature dependency to the diffusion coefficient as well as to the chemical reaction rate constant; a valid procedure as long as the temperature range is not too large (Levenspiel 1972).

$$D_{AB} = D_0 e^{-E_{diff}/RT} \tag{2.54}$$

where D_0 is the equivalent pre-exponential factor for diffusion (cm^2/sec), and

E_{diff} is the activation energy for effective diffusion (kJ/mol).

In their discussion of falsified or disguised kinetics, the previous authors describe that for any n^{th}-order heterogeneous reaction with significant interparticle pore diffusion or external mass transfer resistance, the observed rate of reaction is proportional to $(kD_{AB})^{1/2}$ from the following equation (Froment and Bischoff 1990):

$$(r_A)_{obs} = \frac{S}{V}\sqrt{\frac{2}{n+1}D_{AB}k(C_A)^{(n+1)/2}} \qquad (2.55)$$

where $(r_A)_{obs}$ is the observed rate of reaction (mol/g catalyst/sec),

S is the external surface area of the catalyst (m^2),

V is the catalyst volume (m^3),

n is the reaction order,

D_{AB} is the effective diffusivity (cm^3/cm catalyst/sec),

k is the heterogeneous rate constant (cm^3/g catalyst/sec),

C_A is the molar concentration of the fluid reactant at the solid surface (mol/cm^3).

Equation 2.55 illustrates the dependency of the observed rate of reaction on $(kD_{AB})^{1/2}$. Employing Arrhenius relationships for both the chemical rate constant and the effective diffusion (Eq. 2.53 and 2.54) indicates that the apparent activation energy is the arithmetic average of the activation energies of the intrinsic reaction and diffusion.

$$k_{obs} = \frac{S}{V}\sqrt{\frac{2}{n+1}}\left[D_0 e^{-E_{diff}/RT} k_0 e^{-E_a/RT}\right]^{1/2} \tag{2.56}$$

so that

$$E_{obs} = \frac{d\ln(k_{obs})}{d(1/T)} = \frac{E_{diff} + E_a}{2} \approx \frac{E_a}{2} \tag{2.57}$$

Since the activation energy for gas-phase reactions under chemical reaction control is rather high (80 kJ/mol to 250 kJ/mol) and the activation energy for diffusion is small (5 kJ/mol at room temperature to ~15 kJ/mol at 1000°C (Levenspiel 1972)), Eq. 2.57 is generally true. Therefore, for situations with strong interparticle diffusional or external mass transfer resistance, the observed activation energy may be only one-half the true activation energy. According to Froment and Bischoff (1990), this provides one possible experimental test for the presence of diffusion problems. If the observed activation energy is 20 kJ/mol to 40 kJ/mol, it is probably one-half of the true chemical activation energy value; however, if the observed activation energy is 85 kJ/mol, it could be the true value or one-half of 190 kJ/mol. In this latter instance, the experimental test would be inconclusive.

2.5 Voltammetry

The general electrochemical category of voltammetry includes a sophisticated collection of analytical techniques where the relationship

between voltage and current is observed at an electrode during an electrochemical process. The current measured at the electrode is a function of the potential applied to the electrode and when that potential is systematically varied, the resulting current-potential plot is a voltammogram.

Voltammetry can be used to analyze any electroactive chemical species that can be made to oxidize or reduce. By controlling the electrode potential, the experimenter can control the redox reaction occurring at the electrode surface. Current measured at the electrode surface is a measure of redox electron transfer, or electron flow. This current is proportional to the concentration of electroactive species in the electrochemical system being studied.

Cyclic voltammetry (Harris 1991, Hibbert 1993, Gosser 1994) is used principally to characterize the redox properties of compounds and to study the mechanism of redox reactions. A cyclic potential sweep is imposed on an electrode and the current response is observed. Analysis of the current response can give information about the thermodynamics and kinetics of the electron transfer reaction at the electrode-solution interface, as well as provide information about the kinetics and mechanisms of homogeneous chemical reactions initiated by heterogeneous electron transfer at the electrode surface. A triangular waveform similar to the illustration in Figure 2.4a is applied to the working electrode and the current generated at the

electrode is measured (Figure 2.4b). By convention, an oxidizing potential is assigned a positive value and the associated anodic, or oxidizing current is assigned a negative value. Conversely, a reducing potential is assigned a negative value and its associated cathodic, or reducing current is positive.

For any cyclic voltammogram, the initial sweep potential is set at a value (the rest potential) where zero current occurs (t_0 in Fig. 2.4). This value is generally not at either the cathodic or anodic extreme, but rather at an somewhat arbitrary intermediate value. As the potential sweep begins, for example in the positive anodic direction, the current associated with the anodic redox process increases to a maximum and decreases as the potential is made even more positive. This happens as the electroactive species becomes depleted immediately around the electrode surface, and diffusion from the bulk solution is too slow to replenish the depleted concentration. As the anodic potential reaches its maximum value (t_1 in Fig. 2.4), the current has decayed to a relatively small value. After t_1, the potential is reversed and the sweep begins in the negative cathodic direction.

When the potential is sufficiently reducing, the oxidized species around the electrode begins to reduce and the cathodic wave begins to appear. The cathodic current also passes through a maximum as applied potential decreases and ultimately decays as the potential approaches the maximum cathodic value (t_2). The potential is again reversed, and anodic

potential is applied to achieve the final rest potential (t_0), and the completion of one potential sweep cycle.

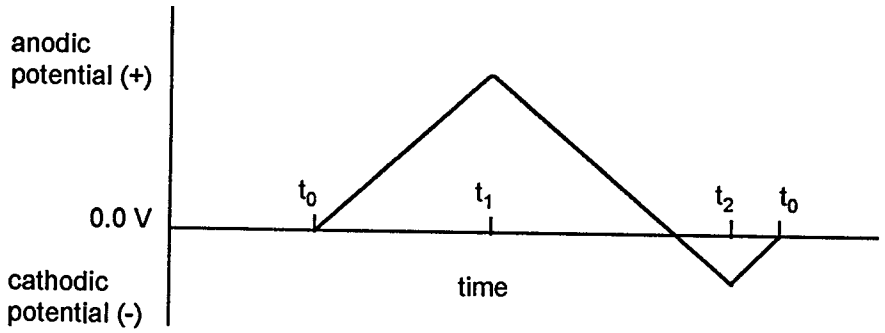

(a)

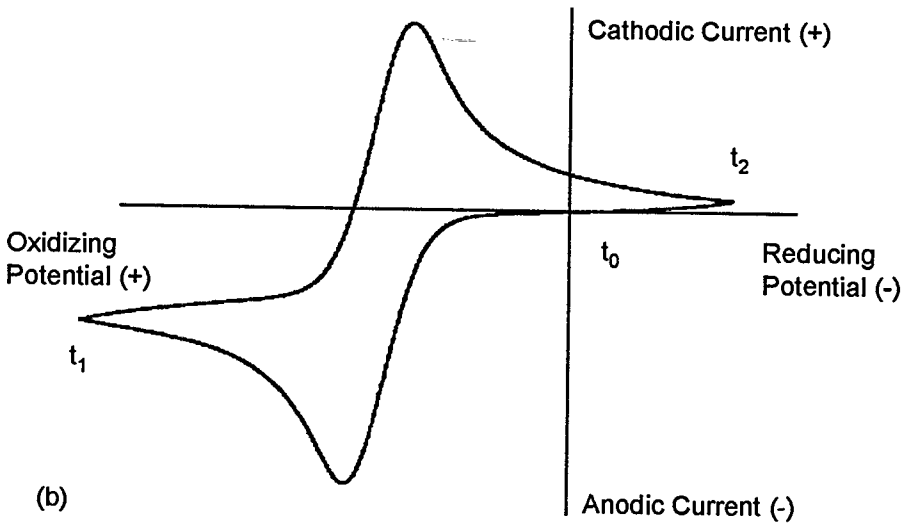

(b)

Figure 2.4. (a) the potential waveform used in cyclic voltammetry, and (b) the resulting cyclic voltammogram.

The voltammogram in Figure 2.4b is an example of a reversible electrode reaction where the redox process is fast enough to maintain equilibrium concentrations of both reactant and product at the electrode surface as the electrode potential is varied. Studying the peak current as a function of the rate of change of applied potential is useful in evaluating the kinetic rate constants of electrochemical reactions. If there are secondary chemical reactions competing for the electrochemical reactants or products, the shape of the voltammogram will reflect the rates of these competing reactions.

2.6 Mixing and Segregation in Dry Particulate Systems

Wide differences among material properties such as particle size distribution, density, particle shape, porosity, and any surface characteristics, such as electrostatic charge or adsorbed moisture, make dry blending or dry segregation of particulate systems very difficult to achieve with consistent uniformity. In fact, powder handling technologists still do not completely understand the interaction of specific material properties well enough to predict the performance of a bulk assemblage without the benefit of laboratory testing or previous field experience. Technologists *do* recognize that materials in dry particulate systems interact; not only among the various size fractions of the same material, but also among other materials present in

the system. However, the *a priori* prediction about the interactive behavior of a specific system in mixing or segregating modes is generally not possible. In some systems, the interaction of the material is so profound that dry material segregation can not be accomplished.

In particular, the properties and behavior of fine powders (<70 μm) are especially interesting. Dry particulate mixing generally follows one of two theories based on the cohesive characteristics of the particle system. The *random mixing theory* (Williams 1968, Hershey 1975) assumes that free-flowing particles similar in size, density, and size distribution are randomly mixed according to a variety of mechanisms including diffusion and convection. The *ordered (or interactive) mixing theory* does not require equally sized or weighted particle distributions and utilizes the natural cohesive or interparticle interaction (adsorption, chemisorption, surface tension, frictional, electrostatic, or other forms of adhesion) to help explain homogeneity in the final particulate system (Hershey 1975, Yip and Hershey 1977a, 1977b, Egermann 1980, Lai et al. 1981).

The concept of ordered mixing is based on adhesion of fine particles to larger particles in the system. These cohesive properties and other surface phenomena tend to develop with increasing particle fineness and have been found to *order* rather than *randomize* the mixing process (Hershey 1975). This has been demonstrated in the pharmaceutical industry where the

importance of complete and uniform mixing of microdose quantities of specific drugs with inert carrier vehicles is important for dosage control and product quality assurance. These studies have been dominated by bi-particulate systems where the mono-size inert carrier particles are of the order of several hundred microns in diameter and the smaller drug particles are <5 to 100 microns in diameter. Ordered mixing is the result of uniform adhesion of the smaller particles to the larger particle, and was found to be present in several cases (Yip and Hershey 1977b, Bryan et al. 1979, Rees and Staniforth 1979, Lai et al. 1981, Ibrahim et al. 1989, Fan and Chen 1990).

Segregation or separation of the smaller particles from the final mixture was found to be achieved, but only to a limited extent based on the pore size of the larger carrier vehicle (Rees and Staniforth 1979), the concentration of the micronized particle fraction (Bryan et al. 1979, Lai et al. 1981), the energy input and bed height of the segregation apparatus (Lai et al. 1981), and from the presence of a size distribution in the larger carrier vehicle (Yip and Hershey 1977a).

The problem of efficient segregation of fine particulate systems has also been studied in gas-fluidized bed applications. As with bulk dry-powder mixing, interparticle forces was found to promote aggregation of fine particles (<70 μm), prevent their uniform dispersion, and result in channeling and

excessive entertainment in the off gas stream. The forces attributed to the cohesion of fine particles included van der Waals forces (Rumpf 1962, Baerns 1966, Chaouki et al. 1985, Bowling 1988, Visser 1989, Lam and Newton 1992, Baeyens 1992); electrostatic attraction (Rumpf 1962, Derjaguin et al. 1968, Bailey 1984, Briens et al. 1992); fluid bridges (Parker and Stevens 1959, Rumpf 1962); and a general crystallization or precipitation phenomena (Geldhart et al. 1984, Kono 1987).

In the work by Chaouki et al. (1985), mixed copper-alumina aerogels initially a few nanometers in size, agglomerated to form secondary and tertiary particles ultimately achieving particles on the order of a micron in diameter. The bulk material was found to be extremely amorphous with a specific surface area of ~400 m^2/g and a bulk density of only 66 kg/m^3. After fluidization above a minimal superficial gas velocity, the particles again agglomerated to form clusters on the order of 1000 μm in size. They postulated a model based on van der Waals forces as responsible for the agglomeration phenomena. In a later work, Li et al. (1990) also found that in high velocity gas-fluidized beds SiO_2 and Fe_2O_3-SiO_2 aerogels originally <20 μm in size agglomerated into stable clusters nominally 200 μm to 300 μm in diameter.

Since material properties, particle size distribution, and the particle environment define the mechanism of agglomeration, fine particle cluster

stability can vary widely. In investigating the role of electrostatic forces on the adhesion of polymer particles to solid surfaces, Derjaguin (1968) determined that it required an acceleration of 10^5-10^6 g to remove small particles (<30 μm) in a direction normal to the substrate surface. Others (Mantz 1988, Ranade et al. 1988, Thoma 1991, Jaraiz 1992) also attempted to quantify interparticle forces and agglomerate strength distributions to understand the fundamental nature of their formation and to develop methods for their dispersion. In many cases, partial to total dispersion of fine particulate systems can be achieved by vibration, the use of ultrasonic or high-decibel acoustic fields, and by the use of liquid media, or by combinations. It was generally concluded by Bowling (1988), however, that by immersing adherent particles in a liquid, the van der Waals force could be reduced by about a factor of two because the liquid shielded the attractive force. It was also determined that electrostatic effects also become negligible because of the larger magnitude of the static dielectric constant of the liquid medium compared to that of a gas or a vacuum.

Briens (1992) used surfactants in an ultrasonic bath to de-agglomerate materials prior to determining their particle size distribution by laser light diffraction. The work by Renade et al. (1988) and the review by Bowling (1988) conclude that for the microelectronics and semiconductor industries, the use of liquid media (possibly in combination with surfactants and

ultrasound) allowed for better cleaning of micron and sub-micron size particles from surfaces; and that non-contact cleaning was much less effective than the action of physical scrubbing.

Generally, in all of these investigations into fine dry powder interaction, some method of particle size determination was performed on the final mixture. In cases where fine particles (<70 μm) were a part of the final mixture, *never was dry sieving used* as the technique for determining the final size distribution. Nathier-Defour et al. 1993, Karuhn 1996, and Nushart 1996 agreed that below ~80 μm, the effectiveness of segregation by dry sieving became questionable. In work by Benoni et al. (1994), wet sieve analysis was performed on the fluidized bed material to determine if agglomerates were contributing to the entrainment flux. Wet sieving was the technique chosen because of its ability to disperse possible fine particle agglomerates in samples collected from the fluid bed off gas stream. Other researchers relied on dry particle image analysis to examine cluster formation, while still others used laser diffraction or sedigraph techniques for determining particle size distributions of fine particle assemblages.